Hindawi
Complexity
Volume 2019, Article ID 7081784, 17 pages
https://doi.org/10.1155/2019/7081784

Research Article

Bidirectional Multi-Input and Multi-Output Energy Equalization Circuit for the Li-Ion Battery String Based on the Game Theory

Jiayu Wang,[1] Shuailong Dai ,[1,2] Xi Chen ,[1] Xiang Zhang,[1,2] and Zhifei Shan[1,2]

[1]*College of Electrical Engineering & New Energy, China Three Gorges University, Yichang, China*
[2]*Hubei Province Collaborative Innovation Center for New Energy Microgrid, CTGU, China*

Correspondence should be addressed to Shuailong Dai; daishuailong@126.com

Received 21 February 2019; Revised 2 May 2019; Accepted 20 May 2019; Published 13 June 2019

Academic Editor: Hassan Zargarzadeh

Energy inconsistency among Li-ion battery cells widely exists in energy storage systems, which contributes to the continuous deterioration of the system durability and overall performance. Researchers have proposed various kinds of battery energy equalizers to reduce such inconsistency. Among them, the inductor equalizer is a predominant type in fast equalization applications. However, it requires relatively more complex control than other types of equalizers. In order to reduce the control complexity of inductor equalizers, a bidirectional multi-input and multi-output energy equalization circuit based on the game theory is proposed in the present work. The proposed equalizer has the modularized circuit topology and the mutually independent working principle. A static game model is developed and exploited for the mathematical description and control analysis of an energy equalization circuit comprised of these equalizers. The feasible control of each equalizer was obtained by solving a series of linear equations for the Nash Equilibrium of the model among the states of charge of the battery cells. The complexity of equations grows linearly with the cell number. The equivalent simulation model for the four-cell equalization is established in the PISM software, where the operational data and simulation results justify the static game model and verify the control validation, respectively. It is concluded that the proposed inductor equalizer is suitable for large-scale battery strings in energy storage systems, electrical vehicles, and new energy power generation applications.

1. Introduction

Li-ion batteries have been extensively used for energy storage systems in electrical vehicles, new energy power generation, and military applications because of their superior performance [1–4]. However, energy inconsistency among the battery cells widely exists in energy storage systems and poses a potential threat to the system safety, which is the major concern of the future applications of the Li-ion batteries [5–8]. Commonly, the cells are assembled into battery strings for instant power supply or energy storage [9]. Some of them might undertake energy inconsistency during recharge cycles and then fall into overcharged or overdischarged state, which can cause cell damaging or even explosion and service life of cells decrease, respectively [10, 11]. Therefore, to ensure the battery service life and the system performance during the charging and discharging periods, the energy equalization of battery strings is mandatory [9, 12]. Many researchers have proposed various battery energy equalizers that each equalizer has distinctive advantages and suitable applications [12–29].

On the one hand, the specific structure of a certain type of equalizer determines its potential performance. Depending on the equalization components and topology, there are generally four types of equalizers: resistor, capacitor, transformer, and inductor equalizers [9]. Resistor shunt equalizers [13, 14] are the simplest type in both control and working principle. The energy of overcharged batteries is consumed by the shunt resistors and dissipated as the resistors heat, which causes notable energy waste and device heating. Its improved type, analog shunt equalizer, causes less energy dissipation and is viable in large-scale battery strings. By contrast,

the equalizers comprised of reactive components perform equalization more efficiently. They redistribute the energy of the battery string by transferring the imbalanced energy with reactive components. Pascual proposed a switched capacitor equalization circuit, where the equalizers alternately connect to adjacent batteries, forming a path to transfer the energy [15]. This circuit is easily controlled and expanded, but the equalizer's current capacity is constrained by the capacitor, which slows down the equalization process. Baughman expanded the second column of capacitors based on Pascual's circuit [16]. Although his work sped up the equalization process by 25%, the capacitance cost increased by 50% [9]. The transformer equalizer is another type of energy carrier. Kyung-Min applied a central transformer to achieve the target energy transfer [17]. The energy of the strong cell is stored by the primary winding and then released to the weak cell from the secondary winding through switch modules. This type of equalizers features in flexible control, but its design is complex and expensive. Moreover, it suffers from saturation. Researchers have been making efforts to improve transformer equalizers. Aiguo Xu spared the switch modules and distributed the secondary winding to each equalizer [18]; Kim divided the primary winding into two stages [19]; S.H Park made a deeper distribution on both the primary and the secondary windings [20]; Xiaolin Wang adopted tapper inductors to form structures like autotransformers [21].

Inductor equalizer is a predominant type in fast equalization, and its design is not as expensive or complex as the transformer equalizer [9]. Nishijima and Kuktut proposed an inductor equalization circuit [22, 23] with similar topology to the switched capacitor circuit, where they replaced capacitors with inductors. This innovation increased the current capacity of equalizers and realized fast equalization. Since there is a shared switch between every two adjacent equalizers, the switch coupling effect results in the complex mathematical description for equalizers. Zhao managed to work out the control for a three-cell battery string [24], but it was complex due to the coupling effect. Yuang-Shung Lee added a resonant loop in the equalizer to reduce the switching loss [25]. Moreover, Cassani analyzed the feasibility of such kind of circuits in the view of the control and concluded that the complexity of the controller exponentially increases as the cell number increases [26]. He gave a compromise solution by dividing the battery cells into several groups to lighten the work of each controller [27]. The potential performance of these inductor equalizers is constrained by inefficient control and their application on the fast equalization is limited to small-scale battery strings. Xiangwei Guo improved the conventional topology and proposed a bidirectional lossless equalization circuit, which features a simple control method and fast balancing. In other words, the proposed circuit has a large equalization current and exhibits outstanding equalization performance [28].

On the other hand, the purpose of equalizer control is to realize the full potential performance of the equalizers. Therefore, working out the control method is essentially a decision problem. Game theory (GT) is the study of utilizing relevant parties in the game of multiple individuals or teams under the constraints of specific conditions and implementing corresponding strategies. It has been studied predominantly as a modeling paradigm in the mathematical social sciences especially in economics [29]. Compared with humanities and economies that cannot be rational, intelligent control seems more suitable to apply the GT [30]. With the development of measurement and control technology, Game Theory has been increasingly applied in system management [31] and resource scheduling [32, 33]. Myerson defined the GT as "a mathematical model for studying conflicts and cooperation between intelligent rational decision makers" [34]. Therefore, in the perspective of control, the GT is a study of conflicts and cooperation between interactive controllers for certain purposes. The controller and purpose are premises of establishing the game model (GM). These two premises are clear in the aforementioned equalization. Equalizers can be regarded as controllers and the purpose is to achieve the energy balance of batteries while for the inductor equalizers mentioned above it is complex to make mathematical descriptions for the equalizers' behaviors, when a considerable number of cells are involved, which becomes a barrier for establishing a mathematical model.

To simplify the control of inductor equalizer, bidirectional multi-input and multi-output energy equalization circuit (BMMEEC) is proposed. The proposed circuit has three characteristics as follows: first, in terms of the circuit topology, each equalizer consists of a dual switch group, connected in a parallel manner with the entire battery string, and an inductor is connected between every two adjacent cells. It should be indicated that no shared switches exist among equalizers; second, in terms of the controllability, each equalizer is controlled independently regardless of the coupling effect; third, in terms of the circuit operation, each equalizer works synchronously; hence the equalization time decreases. Moreover, compared with other types of equalizers, inductor equalizers have a larger current capacity than that from capacitor equalizers. Furthermore, they have lower winding precision requirements than those from transformer equalizers. In the perspective of the circuit modeling, the barrier for the mathematical description is eliminated; equalizers are independent and rational; the mathematical description is feasible and the operational data is measurable. Therefore, the CISGM can be developed and exploited for control analysis, where the equalizers are treated as independent game participants, the battery energy is regarded as the capital of the participants, and the Nash Equilibrium (NE) of the battery energy is set to be the termination of the game. As for the battery energy, it is described by the battery state of charge (SOC) in quantity. SOC is one of the most important parameters in a Li-ion battery, which is usually utilized to reflect the energy state of the battery. Reviewing the literature shows that researchers have proposed variety of accurate methods to investigate the Li-ion batteries [35–39]. The benefit function can be derived to describe participants' behaviors and evaluate the equalization effect.

This paper is organized as follows. In Section 2, the topology and principle of BMMEEC are introduced. In Section 3, the mathematical description of each component of BMMEEC is carried out. It is intended to establish a complete information static game model (CISGM) and

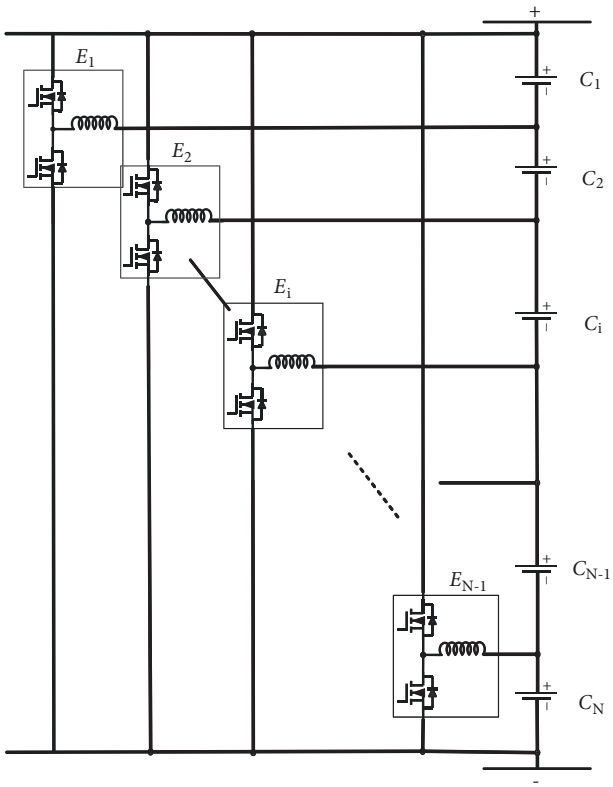

Figure 1: Topology of the BMMEEC.

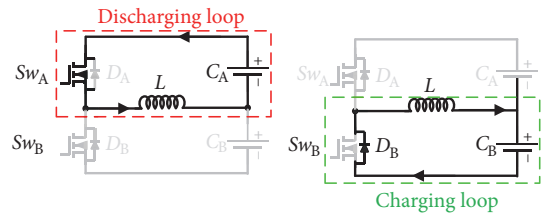

Figure 2: The principle of the equalizer.

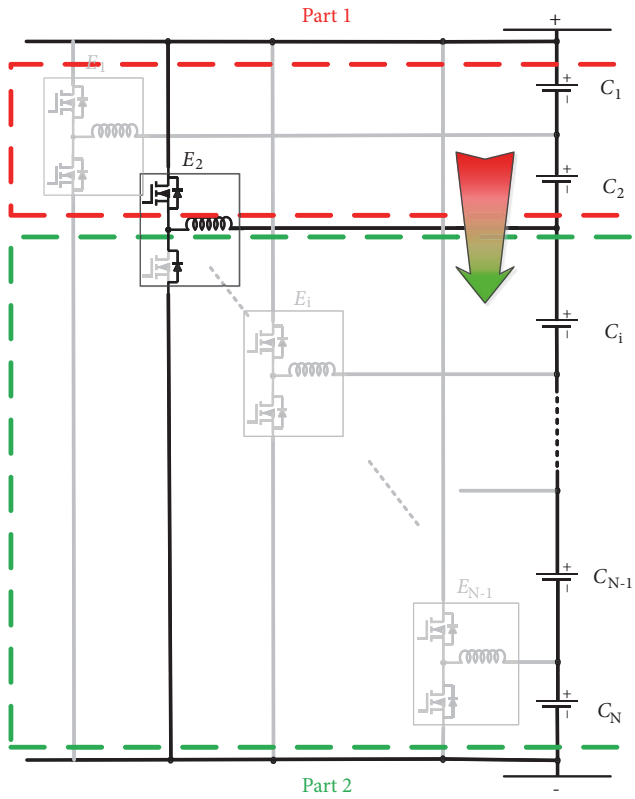

Figure 3: Energy transfer from Part 1 to Part 2, caused by E_n.

derive the benefit function for quantitatively evaluating each equalizer's behavior. The model for a four-cell battery string is established and deduced with the initial SOC of each cell set reasonably. Its solution is transformed into the corresponding control method. In Section 4, simulation results are presented to verify the feasibility of the obtained control. In Section 5, the present work is concluded and the authors' further work is introduced.

2. Topology and Operating Principle

Figure 1 shows the topology of the BMMEEC. It comprises two main parts, equalizers and the battery string. In a certain equalizer, the two switches (MOSFET modules) control the flow of energy and the inductor acts as an energy carrier.

For a battery string that contains N cells, $N-1$ equalizers are needed to conduct the energy equalization. Since each equalizer contains two switches, there are 2^{N-1} kinds of equalizer control combinations. This topology has the following effects: (1) independent equalizers: each equalizer can be independently controlled; (2) overall effect in the energy distribution: any energy transfer caused by a certain equalizer affects the overall energy distribution in the battery string because all the cells are involved.

Figure 2 illustrates the principle of the BMMEEC. During the operation cycle of the equalizer, only one of the two switches can work; otherwise, the cell will be short-circuited.

Figure 2 presents the discharging loop with a red dash line. In this loop, the energy from batteries flows through the actuated switch to the inductor. When the switch is turned on, it forms a discharging loop together with the inductor and the cell above the inductor. Moreover, when the actuated switch is turned off, it forms a charging loop with the inductor and the cell below the inductor, and the energy stored in the inductor is released to the cell below the inductor. Therefore, the energy transfers from batteries above the inductor to batteries below the inductor. Invert energy transfer can be realized in a similar way.

Consequently, in a battery string, energy redistribution for multiple cells is realized as is shown in Figure 3. It is feasible to achieve energy equality for all cells in the battery string by applying proper control for equalizers.

In order to fully utilize the flexible topology of BMMEEC to achieve energy redistribution, it is necessary to mathematically describe and analyze its energy equalization process. Considering the following reasons, it is concluded that the game theory (GT) has high relevance and correspondence to

such flexibility. (1) Independent players: in a game, players independently choose their own strategies to maximize their own benefits. (2) The comprehensive effect in benefit distribution: since all players are involved in the game, any behavior of a certain player affects the balance of the benefit. Moreover, the goal of the players is to maximize the benefit. Therefore, once they cannot get any more benefits, the game comes to the end. According to such relevance and correspondence, it is reasonable to establish a GM for the BMMEEC.

3. Comprehensive Information on the Static Game Model

3.1. Model Assumptions. In order to simplify the model, four assumptions are made as follows.

(1) The design parameters of each cell are identical, such as the value of discharging current, discharging efficiency, battery capacity, and, most importantly, the unique correlation between the SOC and the energy. Therefore, the energy state of each cell is presented by its SOC value.

(2) The initial SOC of each cell is instantly available.

(3) Inductors have enough large inductance, i.e., enough capacity to store the energy from cells.

(4) Energy loss in the equalization process is negligible and all power components work ideally.

3.2. Model Factors

3.2.1. Players: Independent Equalizers. Each equalizer is treated as an independent player. For equalizer E_n, its inbuilt inductor divides the battery string into two parts, the cells above the inductor and the cell below the inductor. ${S_{An}}^0$, S_{An}, and ΔS_{An} are the initial SOC of cells above the inductor, the final SOC of cells, and the SOC difference of batteries, respectively. Furthermore, the related values of cells below the inductor, ${S_{Bn}}^0$ and S_{Bn}, are set similarly. Therefore, (1) can be developed to describe the energy transfer between these two parts caused by the equalizer E_n:

$$\begin{aligned} S_{An} &= {S^0}_{An} + \Delta S_{An} \\ S_{Bn} &= {S^0}_{Bn} + \Delta S_{Bn} \end{aligned} \tag{1}$$

3.2.2. Strategy: Equalizer Control Plans. In a game, the strategy is the combination of all behaviors conducted by players. In this GM, the "behavior" of each equalizer is presented as the implementation of its control plan, which is the conducting time of the actuated switch. For the equalizer E_n, the conducting time of its switch above the inductor and the switch below the inductor is set to t_{An} and t_{Bn}, respectively. Furthermore, its control plan can be described by

$$T_n = \{t_{An}, t_{Bn}\} \tag{2}$$

The control strategy of the game is the combination of control plans for all equalizers:

$$T = \{t_{A1}, t_{A2}, \cdots t_{A(N-1)}, t_{B1}, t_{B2}, \cdots t_{B(N-1)}\} \tag{3}$$

3.2.3. Order: Static Game. In a static game, once the behavior of each player is determined, the game result is determined. In this GM, each equalizer operates with a fixed control plan during the whole game.

3.2.4. Information: Complete Information. In a complete information game, each player has accurate information about other players' characteristics, strategy, and benefits. According to the second assumption of this GM, the initial SOC of each cell is known as the given condition.

3.2.5. Benefits Function. In this game, benefit evaluates the effect of a player's behavior. In other words, proper behavior can maximize a player's benefit. In this GM, the goal of the whole equalization process is to equalize the SOC (S_i) among all the cells. For equalizer E_n, it gets the maximum benefit when the ratio of S_{An} and S_{Bn} is equal to the ratio of the numbers of cells above and below the inductor. The benefits function of equalizer E_n are defined as

$$u_n = -\left|\frac{n}{N-n} - \frac{S_{An}}{S_{Bn}}\right|, \quad n \in [1, N-1] \tag{4}$$

In (4), the absolute value of the difference between two fractions describes the departure of the present SOC distribution from the equalization goal. The departure is used to evaluate the benefit of each equalizer. When equalization results match the goal, the benefit is zero. Note that (4) is always less than 0 in value. Thus, the following inequality always holds:

$$u_n \le 0 \tag{5}$$

3.3. Nash Equilibrium. NE is a strategy with which all players get their maximum benefit. This situation is equivalent to the SOC equality of the battery string. According to the definition of the NE, when it is applied, each player gets the maximum benefit "0" so that (6) can be derived as [25]

$$\begin{aligned} &u_n\left({t_{A1}}^*, {t_{B1}}^*, \ldots {t_{A(N-1)}}^*, {t_{B(N-1)}}^*\right) \\ &\quad \ge u_n\left({t_{A1}}^*, {t_{B1}}^*, \ldots t_{An}, t_{Bn}, {t_{A(N-1)}}^*, {t_{B(N-1)}}^*\right) \end{aligned} \tag{6}$$

where $t_{A,n}$ and $t_{B,n}$ are the best strategy for the equalizer E_n, called ${t_{A,i}}^*$ and ${t_{B,i}}^*$, $i \in [1, n) \cup (n, N]$. Moreover, it is obvious that the value of benefit function is always less than or equal to zero and (7) can be derived:

$$u_n \ge 0 \tag{7}$$

NE is the solution of the GM and, in order to figure it out, the equivalent equation group is derived from the two inequalities:

$$u_i = 0 \quad (i = 1, 2 \ldots N-1) \tag{8}$$

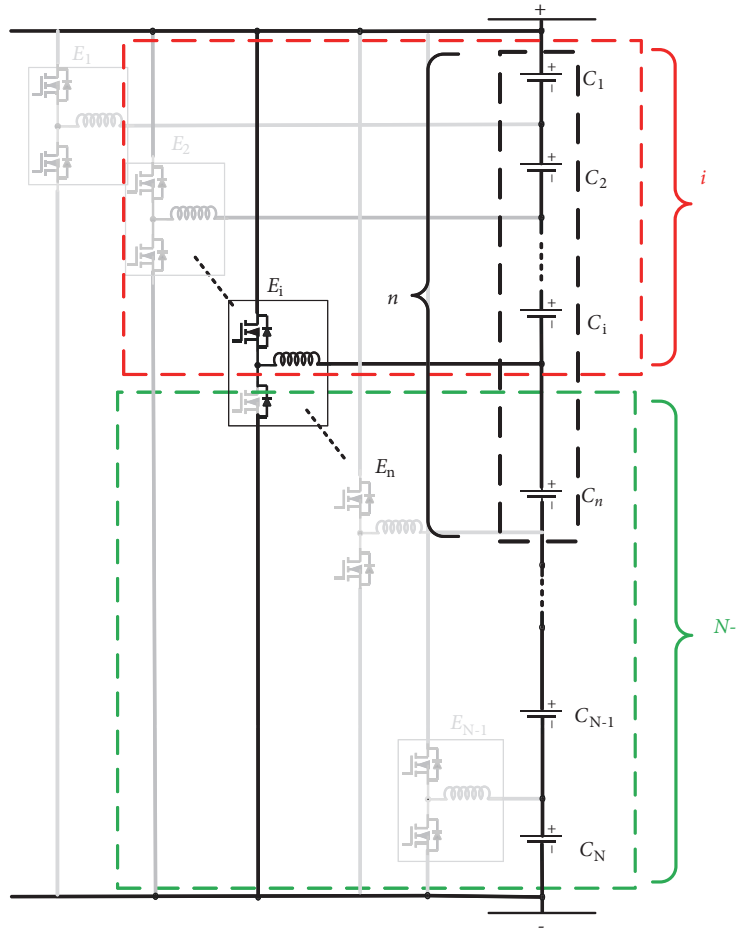

Figure 4: Energy transfer caused by the equalizer E_i in the situation I.

Substituting S_{An} and S_{Bn}, (8) is expressed in a more specific form:

$$\begin{aligned}
\Delta S_{A1} &= \overline{S} - S^0{}_{A,1} \\
\Delta S_{A2} &= 2\overline{S} - \left(S^0{}_{A1} + S^0{}_{A2}\right) \\
\Delta S_{A3} &= 3\overline{S} - \left(S^0{}_{A1} + S^0{}_{A2} + S^0{}_{A}\right) \\
&\vdots \\
\Delta S_{A(N-1)} &= (N-1)\,\overline{S} - \sum_{i=1}^{N-1} S^0{}_{Ai}
\end{aligned} \tag{9}$$

In (9), $\overline{S}$ is the mean value of the initial SOC of all cells. According to the second assumption, except for the SOC divergence ΔS_{An}, all values are known as given data.

3.4. The Expression of SOC Divergence. Applying the amperometric method, the SOC difference of a single cell can be expressed as the integral of its discharging time [32]:

$$\Delta S = \int_0^t \frac{\eta I}{C} \mathrm{d}t \tag{10}$$

where I, η, and C denote the discharging current, discharging efficiency, and the capacity of the cell, respectively. According to the first assumption, the design parameters of all cells are identical. In an extremely short period, the cell discharging current I is considered as a constant. Therefore, the three coefficients, I, η, and C, can be presented by one, k:

$$\Delta S = kt_{Discharging} \tag{11}$$

where ΔS_{An} describes the overall SOC divergence for the selected n cells above the inductor of the equalizer E_n. Note that k is determined by the battery string itself, while ΔS_{An} is determined by all other equalizers' control plans. For the sake of universality, the equalizer E_i is chosen to represent the equalizers other than E_n. In the following four situations, the n cells are selected as research objects to study the influence caused by different equalizer on their SOC. The discharging loops and charging loops are framed with red dash lines and green dash lines, respectively.

3.4.1. Situation I. Figure 4 shows the discharging and charging loops distributed by the equalizer E_i when $i \leq n$ and the switch above the inductor is actuated. The discharging time of the cells in the discharging loop is presented by the switch conducting time (t_{Ai}). When the switch is on, the cells in the

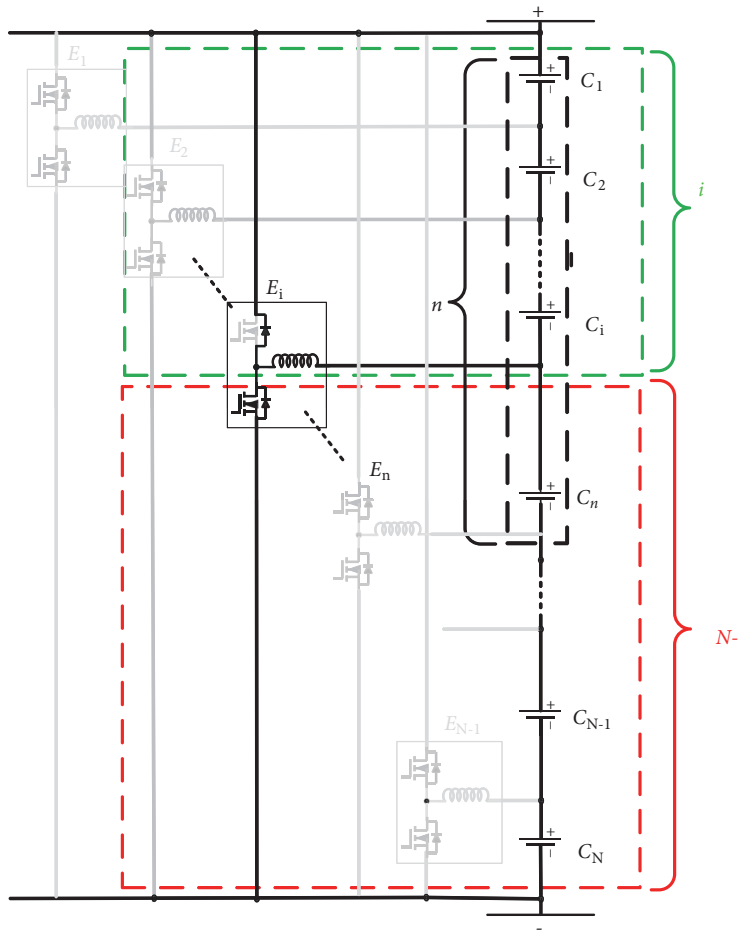

Figure 5: Energy transfer caused by the equalizer E_i in situation II.

discharging loop charge the inductor, and the SOC difference of the selected n cells is described as

$$\Delta S_{An,i}^{(1)} = -i \times k \times t_{Ai} \tag{12}$$

On the other hand, when the switch is off, the energy stored in the inductor is released to all cells in the charging loop, and $i(n-1)/(N-1)$ of the released energy flows to the $(n-1)$ cells included in the selected n cells. Therefore, the SOC difference of the selected n cells in this process is

$$\Delta S_{An,i}^{(2)} = \frac{i}{N-i}(n-i) \times k \times t_{Ai} \tag{13}$$

3.4.2. Situation II. Figure 5 illustrates the discharging and charging loops distributed by the equalizer E_i when the switch below the inductor is actuated. The discharging time of the cells in the discharging loop is presented by the switch conducting time (t_{Bi}). When the switch is on, $(N-i)$ cells in the discharging loop charge the inductor. During this process, the SOC difference of selected n cells is

$$\Delta S^{(3)} = -(n-i) \times k \times t_{Bi} \tag{14}$$

Similarity, when the switch is off, the energy stored in the inductor is released to cells that are all included in selected n cells and the SOC divergence of the selected n cells in this process is

$$\Delta S^{(4)} = (N-i) \times k \times t_{Bi} \tag{15}$$

In summary, when $i \le n$, the SOC divergence of selected n batteries caused by the equalizer E_i is the sum of the SOC difference in four processes:

$$\Delta S_{An,i}{}' = \Delta S_{An,i}^{(1)} + \Delta S_{An,i}^{(2)} + \Delta S_{An,i}^{(3)} + \Delta S_{An,i}^{(4)} \tag{16}$$

3.4.3. Situation III. When $n < i \le N-1$, the selected n batteries are all included in either discharging or charging loops, determined by the equalizer E_i. Figure 6 shows the discharging and charging loops when the switch above the inductor is actuated. When the switch is on, the cells in the discharging loop charge the inductor, and the SOC divergence of the selected n cells is described as

$$\Delta S_{An,i}^{(5)} = -n \times I \times t_{Ai} \tag{17}$$

When the switch is off, the stored energy in the inductor is released to all cells in the charging loop but they are excluded from selected n cells. There is no SOC divergence of selected n cells.

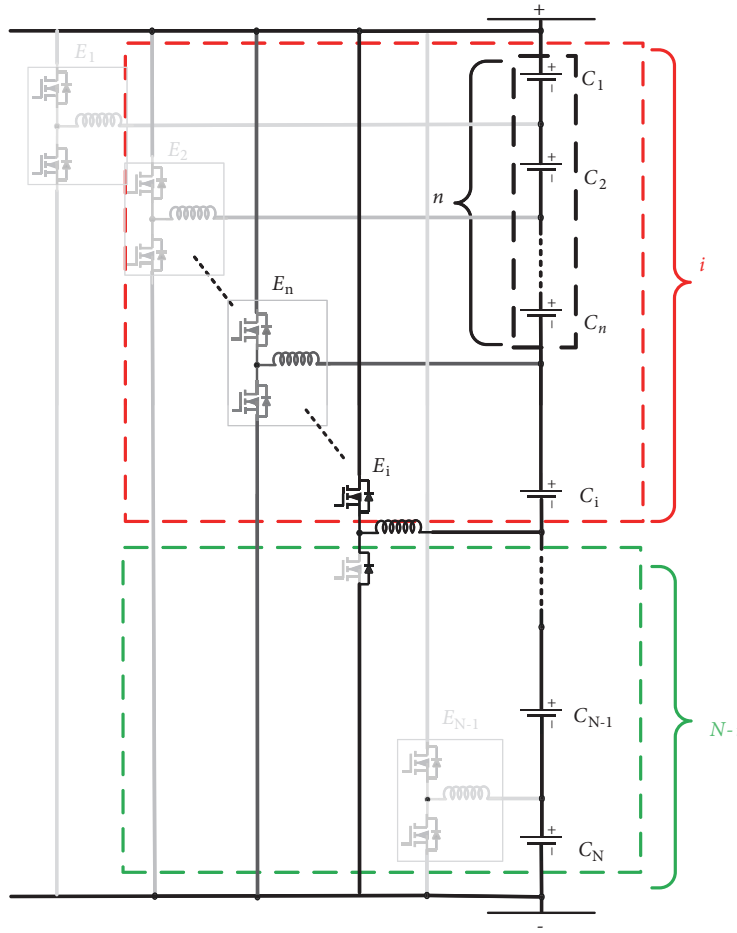

Figure 6: Energy transfer caused by the equalizer E_i in situation III.

3.4.4. Situation IV. Figure 7 illustrates the discharging and charging loops caused by the equalizer E_i when the switch below the inductor is actuated. When the switch is on, $(N-1)$ cells in the discharging loop charge the inductor. In this process, there is no SOC divergence of selected n cells.

When the switch is off, the stored energy in the inductor is released to the cells in the charging loop and n/i of the cells are included in the loop. The SOC divergence of selected n cells is

$$\Delta S_{An,i}^{(6)} = \frac{n}{i}(N-i) \times k \times t_{Bi} \tag{18}$$

In summary, when $n < i \le (N-1)$, the SOC divergence of the selected n cells caused by the equalizer E_i is the sum of the SOC divergence in the two processes:

$$\Delta S_{An,i}'' = \Delta S_{An,i}^{(5)} + \Delta S_{An,i}^{(6)} \tag{19}$$

According to the analysis above, the SOC divergence caused by one certain equalizer E_i is

$$\begin{aligned}\Delta S_{An,i} &= \Delta S_{An,i}' + \Delta S_{An,i}'' \\ &= kI\left\{\left[-i + \frac{i}{N-i}(n-i) - n\right]t_{Ai}\right. \\ &\left. + \left[-(n-i) + (N-i) + \frac{n}{i}(N-i)\right]t_{Bi}\right\}\end{aligned} \tag{20}$$

The final expression of ΔS_{An} is the sum of the SOC divergence, caused by all equalizers on the selected n cells:

$$\begin{aligned}\Delta S_{An} = kI\left\{\sum_{i=1}^{n}\left[\left(\frac{-i(N-n)}{N-i}\right)t_{Ai}\right] + \sum_{i=n+1}^{N-1}(-nt_{Ai})\right. \\ \left. + \sum_{i=1}^{n}\left[(N-n)t_{Bi}\right] + \sum_{i=i+1}^{N-1}\left[\frac{n(N-i)}{i}t_{Bi}\right]\right\}\end{aligned} \tag{21}$$

Equation (21) indicates that the expression is a function of control strategy variables, t_A, t_B. The coefficients are determined by the number of batteries contained in the battery string. For the sake of expression convenience, a coefficient matrix K is set to present coefficients and its specific form is shown in Table 1.

Table 1: Elements in the coefficient matrix K.

K	t_{A1}	t_{A2}	t_{A3}	$\cdots$	$t_{A(N-1)}$	t_{B1}	t_{B2}	t_{B3}	$\cdots$	$t_{B(N-1)}$
ΔS_{A1}	-1	-1	-1	$\cdots$	-1	$N-1$	$\frac{N-2}{2}$	$\frac{N-3}{3}$	$\cdots$	$\frac{1}{N-1}$
ΔS_{A2}	$-\frac{N-2}{N-1}$	-2	-2	$\cdots$	-2	$N-2$	$N-2$	$\frac{2(N-3)}{3}$	$\cdots$	$\frac{1}{N-1}$
ΔS_{A3}	$-\frac{N-3}{N-1}$	$-\frac{2(N-3)}{N-2}$	-3	$\cdots$	-3	$N-3$	$N-3$	$N-3$	$\cdots$	$\frac{3}{N-1}$
ΔS_{A4}	$-\frac{N-4}{N-1}$	$-\frac{2(N-4)}{N-2}$	$-\frac{3(N-4)}{N-3}$	$\cdots$	-4	$N-4$	$N-4$	$N-4$	$\cdots$	$\frac{4}{N-1}$
$\vdots$	$\vdots$	$\vdots$	$\vdots$	$\vdots$	$\vdots$	$\vdots$	$\vdots$	$\vdots$	$\cdots$	$\vdots$
$\Delta S_{A(N-1)}$	$-\frac{1}{N-1}$	$-\frac{2}{N-2}$	$-\frac{3}{N-3}$	$\cdots$	$-(N-1)$	1	1	1	$\cdots$	1

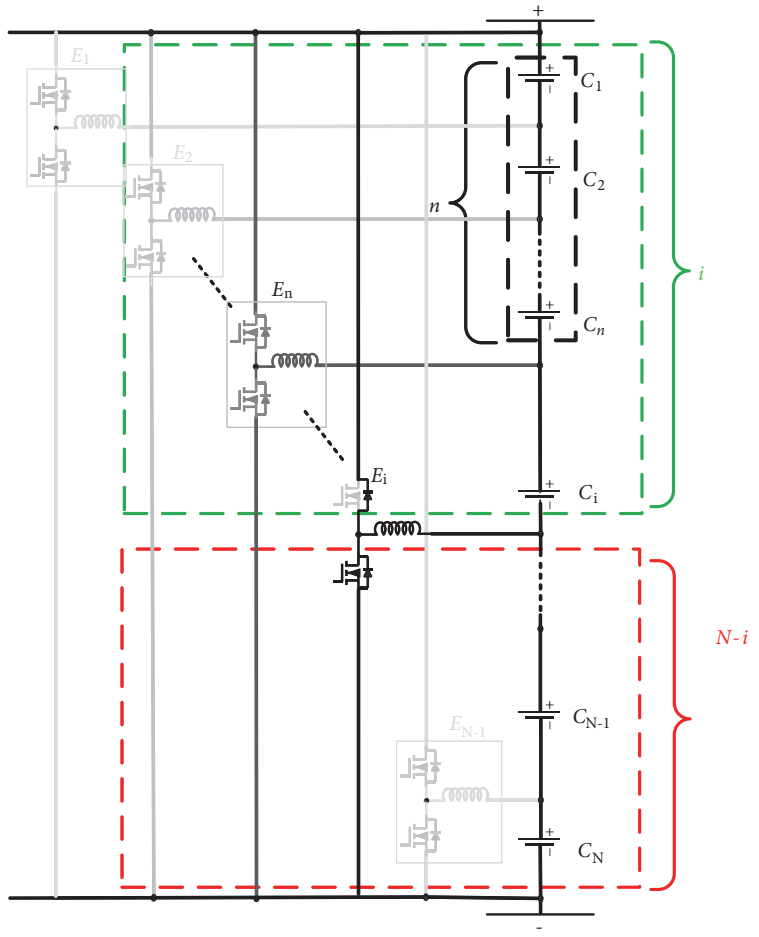

Figure 7: Energy transfer caused by the equalizer E_i in situation IV.

3.5. Solution and Control. For the sake of expression convenience, the SOC divergence in (9) is also presented by a matrix ΔS. By substituting initial SOC values of all batteries, the matrix in the form of (9) can be derived:

$$\Delta S = KT \tag{22}$$

In (21), K, $[K, \Delta S]$, and T are the coefficient matrix, the augmented matrix, and the column vector of independent control variables, respectively. The rank of K and $[K, \Delta S]$ matrices is $(N-1)$, which is always less than the number of independent variables, $2(N-i)$. Therefore, the solution is infinite. The general solution is expressed by (23), which consists of $(N-1)$ set of linearly independent solution vectors $\beta_1 \cdots \beta_{N-1}$ and one special solution β_0 for given initial values:

$$T = c_1\beta_1 + c_2\beta_2 + \cdots c_{N-1}\beta_{N-1} + \beta_0 \tag{23}$$

Although the solution is infinite, only one feasible solution has the corresponding control strategy. Feasible requirements are as follows.

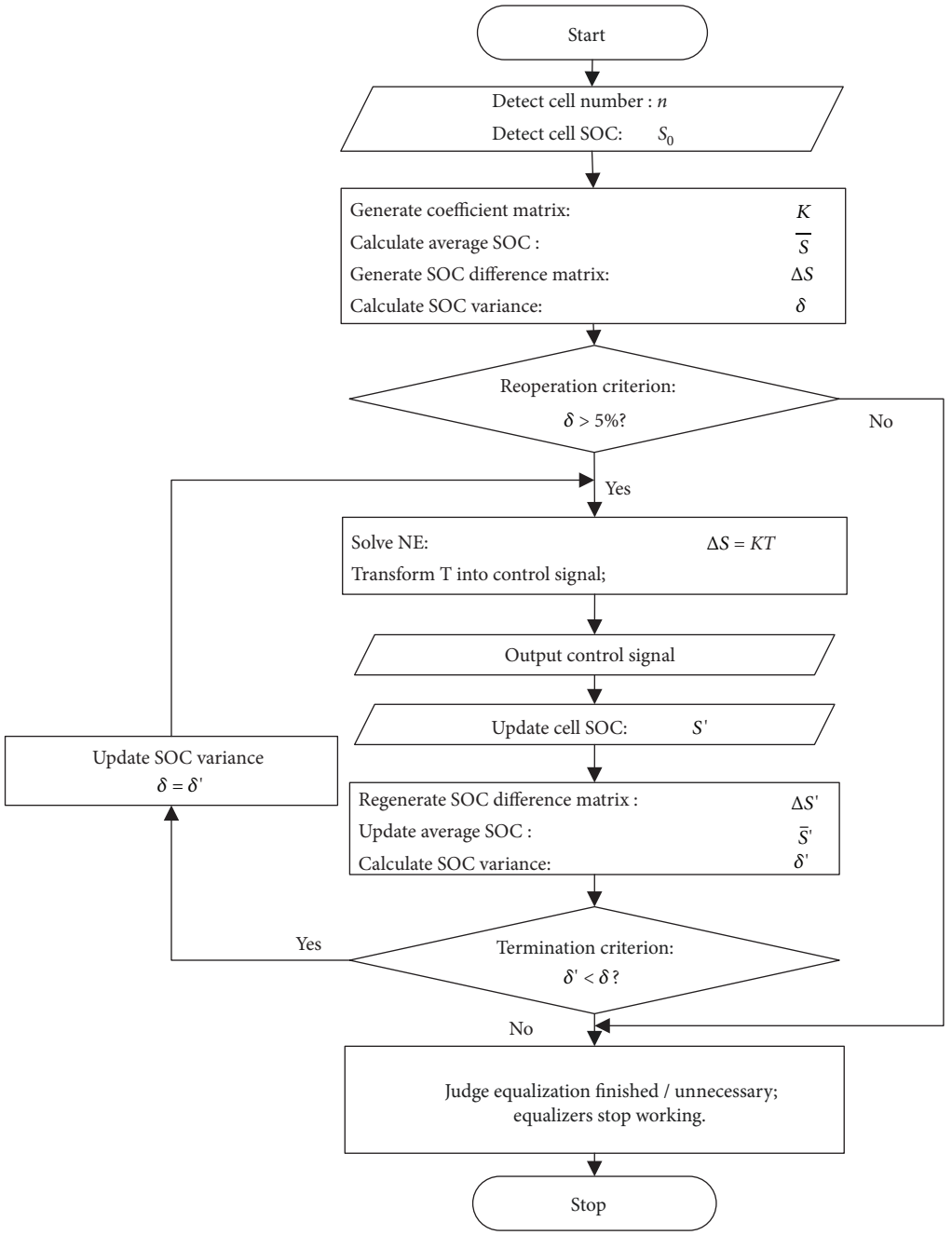

Figure 8: Flowchart of equalizer control algorithm.

(1) Switch conducting time cannot be negative.

(2) Only one of two switches in an equalizer can be actuated. Otherwise, part of batteries in the battery string may be short-circuited. In other words, the product of t_{Ai} and t_{Bi} must be zero.

With these two requirements, the feasible solution can be uniquely determined. According to the feasible solution, the control strategy can be realized by setting the proper duty cycle of three corresponding switches:

$$\alpha_{A1}:\alpha_{A2}:\cdots\alpha_{A,(N-1)}:\alpha_{B1}:\alpha_{B2}:\cdots\alpha_{B,(N-1)} = T \quad (24)$$

3.6. Equalizer Control Algorithm. In the BMMEEC, each equalizer exchanges the energy between upper and lower parts of cells, independently. It should be indicated that the energy equality of each cell in the battery string is the main goal of each equalizer. The control algorithm of the BMMEEC is illustrated in Figure 8. Ignoring the process of the other parts of the equalization system, the BMMEEC controller algorithm can be explained in the following steps.

Step 1. The system detects the basic input parameters of the CISGM, the scale of the battery string (n), and the initial state of charge of cells (S_0).

Step 2. The processor calculates the coefficient matrix (K), average SOC ($\overline{S}$), difference matrix of the SOC (ΔS), and variance of the SOC (δ) to form the NE equations.

Step 3. If the SOC variance exceeds 5%, the system conducts the equalization procedure.

Step 4. The processor solves linear equations to work out the NE of the static game model (T) and transforms it into control signals.

Step 5. The controller outputs the signal to equalizers to actuate the MOSFETs.

Step 6. The system redetects S_0 after the first round of the equalization.

Step 7. The processor calculates $\overline{S}$, ΔS, and δ accordingly.

Step 8. System conducts the termination judgment. If the SOC variance decreases after the first round of equalization, the process will return to Step 4. This procedure is repeated until the variance reaches its minimum value.

Step 9. The termination criterion is met and the equalizers stop.

4. Simulation

4.1. Control Strategy. Taking a battery string that contains four cells, for example, the initial SOC of four batteries are set to be 0.86, 0.91, 0.93, and 0.90. Substitute the number of cells $N = 4$ and initial SOC values into (21):

$$\begin{bmatrix} -1 & -1 & -1 & 3 & 1 & \frac{1}{3} \\ -\frac{2}{3} & -2 & -2 & 2 & 2 & \frac{2}{3} \\ -\frac{1}{3} & -1 & -3 & 1 & 1 & 1 \end{bmatrix} T = \begin{bmatrix} 4 \\ 3 \\ 0 \end{bmatrix} \tag{25}$$

The general solution of (25) is obtained as

$$T = c_1 \begin{bmatrix} 3 \\ 0 \\ 0 \\ 1 \\ 0 \\ 0 \end{bmatrix} + c_2 \begin{bmatrix} 0 \\ 1 \\ 0 \\ 0 \\ 1 \\ 0 \end{bmatrix} + c_3 \begin{bmatrix} 0 \\ 0 \\ \frac{1}{3} \\ 0 \\ 0 \\ 1 \end{bmatrix} + \begin{bmatrix} 0 \\ -1 \\ \frac{3}{4} \\ \frac{5}{4} \\ 0 \\ 0 \end{bmatrix} \tag{26}$$

According to the first feasible requirement, $t_{A,2}$ cannot be negative. Therefore, three coefficients must be properly set to eliminate the negative value. Moreover, according to the second feasible requirement $t_{A,i} \times t_{B,i} = 0$. Therefore, the coefficient c_2 is set to be 1, while other coefficients are set to be 0. The only feasible solution is obtained:

$$T = \begin{bmatrix} 0 & 0 & \frac{3}{4} & \frac{5}{4} & 1 & 0 \end{bmatrix}^{\mathrm{T}} \tag{27}$$

Table 2: Simulation parameters of four-cell battery string.

Parameters	Value
Gating signal frequency	4000Hz
Battery rated capacity	5.4 Ah
Battery discharging current	1.7A
Battery rated voltage	3.7V
The inductance of each equalizer	500uH
Initial SOC of $Cell_1$	0.86
Initial SOC of $Cell_2$	0.91
Initial SOC of $Cell_3$	0.93
Initial SOC of $Cell_4$	0.90

Therefore, the control can be implemented by setting the ratio among the duty cycles of the switches, Sw_{A3}, Sw_{B1}, and Sw_{B2}, to be 3 : 5 : 4.

4.2. Simulation Platform. In order to verify the feasibility of the obtained control strategy, a BMMEEC for the battery string that contains four cells is established in the PISM simulation software. Figure 9 shows the schematic of BMMEEC. The simulation parameters are listed in Table 2.

Figure 9 indicates that the ammeter I1 measures the charging current of the cell C_1. The positive value indicates that the current flows into the battery B_1 and the battery is charging, while the negative value indicates that the current flows away from the cell C_1 and the battery is discharging. Ammeters I2, I3, and I4 measure the discharging currents of cells C_2, C_3, and C_4, respectively. The positive value indicates that the current flows away from the battery and the battery is discharging, while the negative value indicates that the current flows into the battery and the battery is charging. Since only Sw_{B2} and Sw_{A3} switches are actuated, their conduction angles are 100 degrees and remaining switches are presented by antiparallel diodes. Voltmeters connected to Li-ion battery modules detect their SOC in real time. The unmentioned symbols such as O1, D1, and IN1 represent the basic switch components and signal ports for equalizer control. The current waveforms in one cycle detected by the ammeters are illustrated in Figure 10, and the current data is shown in Table 3.

4.3. Results and Analysis. The waveforms of current measured by ammeters in one operation cycle reflect SOC variations of four cells. Figure 10 shows the waveforms of charging and discharging currents of cells in one switch operation cycle. The slope of the current varies with the number of on-off switches. It should be indicated that $t_{A,3}$, $t_{B,2}$, and $t_{B,1}$ are on-off periods of Sw_{A3}, Sw_{B2}, and Sw_{B1} switches, respectively.

In the period from 3.97998s to 3.98004s ($t_{A,3}$), all three switches are turned on, and they form three discharging loops. Under the superposition of the energy transfer effect caused by three switches, cells C_1, C_2, C_3, and C_4 are discharged to the inductor and the discharging speed can be determined by the slope of the current waveform.

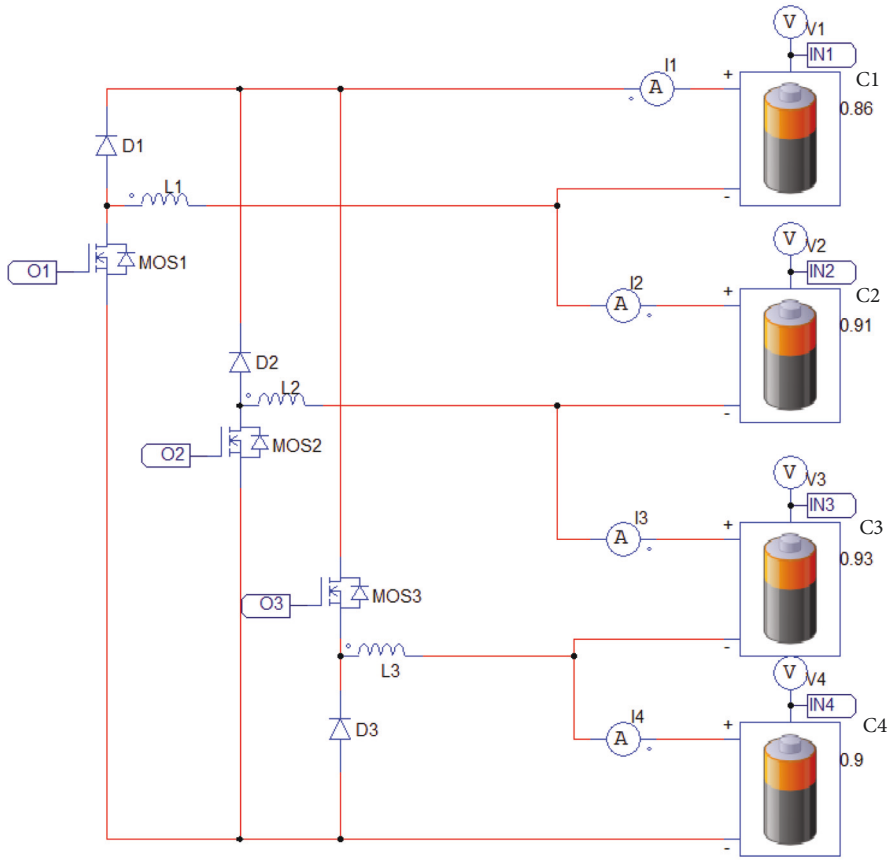

Figure 9: Schematic diagram of the energy equalization circuit.

In the period from 3.98004s to 3.98006s, two discharging loops are formed by switches Sw_{b2} and Sw_{b1}. Moreover, switch Sw_{a3} is turned off to form a charging loop. The decrease of discharging loops leads to the decrease of the amplitude and slope of the discharging current. Furthermore, battery C_1 gradually transformed from the discharging mode to the charging mode.

In the period from 3.98006s to 3.98008s, only Sw_{B1} switch is turned on to form a discharging loop and other two switches are turned off to form two charging loops. It is observed that the discharging speed of C_2, C_3, and C_4 cells further decreases. Moreover, C_2 and C_4 cells gradually enter the charging state. The charging speed of the C_1 cell further increases.

In the period from 3.98008 to 3.90024s, all switches are turned off and there is only one discharging loop in the circuit. The amount of electricity stored in the inductor is released to the battery through the discharging loop. Since this process has nothing to do with the control, so no specific analysis is made for this part. The current integrals are shown in the last column of Table 3; they can present the SOC change of each battery in one operation cycle. In this simulation, the sum of SOC changes of four batteries is slightly greater than zero, because a small part of the power has not been released before the next operation cycle.

After several operation cycles, the four cells power consumption gradually conforms to each other. Figure 11 illustrates the waveform of the SOC in the idle state.

4.4. Comparison with Another Equalization Circuit. In order to investigate the advantages of the BMMEEC, results are compared with those from the inductor-based bidirectional lossless equalization circuit [23] which has high controllability and large current capacity.

Figure 11 demonstrates that the SOC of four cells increases or decreases directly to the final point of the equalization. The unnecessary balancing process in [23] is avoided. Figure 12 is a comparison of simulation results between BMMEEC and the circuit in [23].

In Figure 12, the waveform of the cell voltage or cell SOC reflects the cell energy variation. It should be indicated that the comparison item is the equalization process. Therefore, only the curve of the cell voltage in Figure 11 is taken into account and other factors are out of concern. Figure 12(a) demonstrates that the SOC of four cells increases or decreases directly to the final point of the equalization. Figure 12(b) indicates that the equalization in [23] is achieved in two stages, which means two criterions are needed for the controller to change control command. Moreover, $cell_2$ is discharged in Stage 1 and is charged then in Stage 2, which results

Table 3: Balancing current in one operation cycle for the ideal gating signal.

Current(A)	Time(s)							$\int_0^T Idt$ (A∗s)
	3.97998	3.98004	3.98006	3.98008	3.98010	3.98017	3.98024	
I1	0.381	-0.8764	7.3586	2.3505	1.6895	1.0261	0.3758	-1.63e-4
ΔI1	0	-1.2574	8.235	-5.0081	-0.6110	-0.6634	-1.9747	
I2	3.61e-6	2.0959	1.0438	-0.471	-4.58e-2	3.64e-6	3.61e-6	7.49e-5
ΔI2	0	2.0959	-1.0521	-1.5148	0.4252	0.0458	0.471	
I3	3.51e-6	2.6398	1.7257	0.0004	4.56e-6	3.54e-6	3.51e-6	5.28e-5
ΔI3	0	2.6398	-0.9141	-1.7253	-4.00e-4	-1.02e-6	-3.96e-4	
I4	2.68e-6	1.7566	0.8996	-0.7335	-0.5326	-6.42e-4	2.67e-6	8.65e-5
ΔI4	0	1.7566	-0.8570	-1.6331	0.2009	0.5262	0.734	

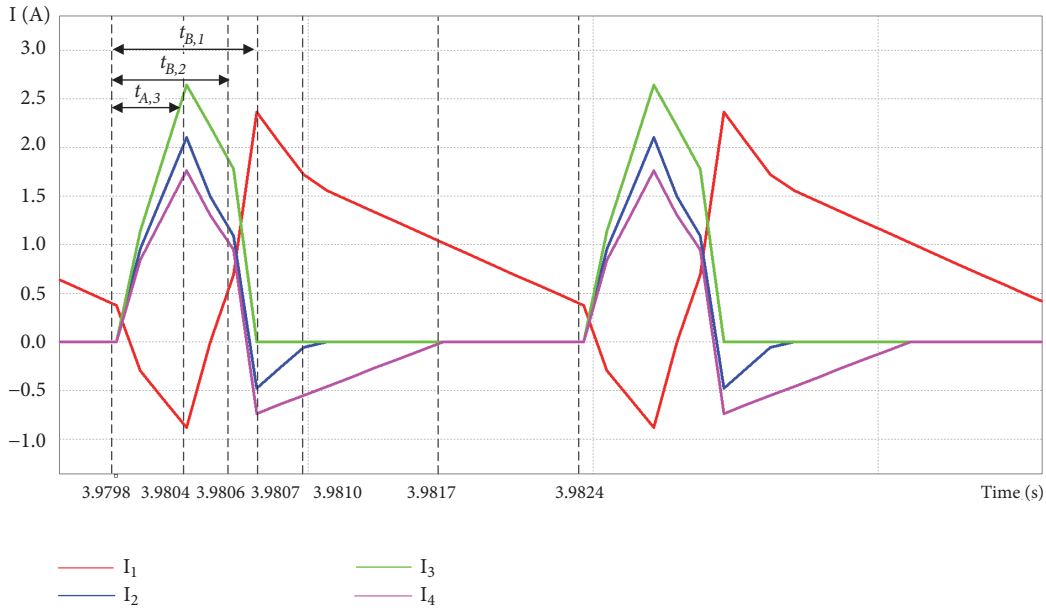

Figure 10: Waveform of the current measured by I1, I2, I3, and I4.

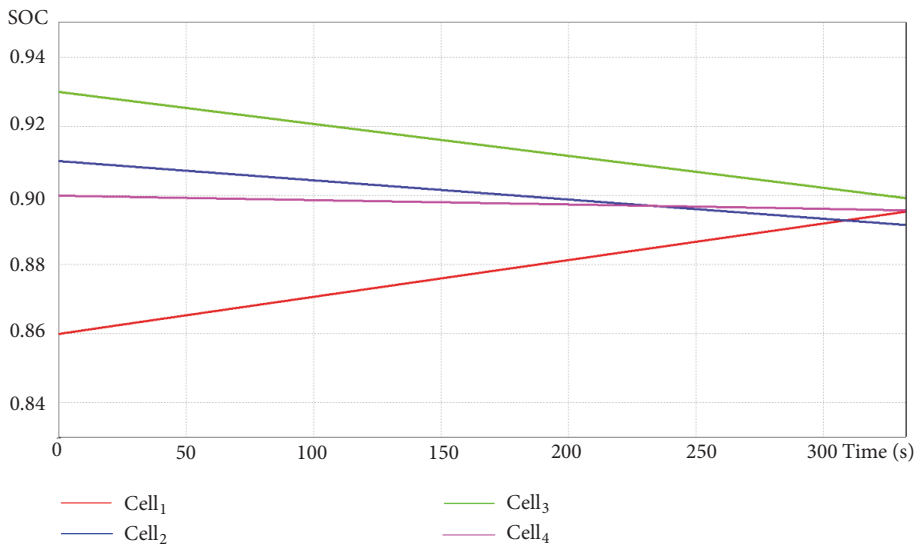

Figure 11: SOC waveform for the ideal gating signal.

Table 4: Comparison of equalization results in three states.

SOC	Initial state (%)	Idle state (%)	Charging state (%)	Discharging state (%)
C_1	86.00	88.91	91.91	85.71
C_2	91.00	88.30	91.16	85.14
C_3	93.00	89.73	92.55	86.60
C_4	90.00	88.68	91.62	85.48
Variance	8.67	0.36	0.34	0.39

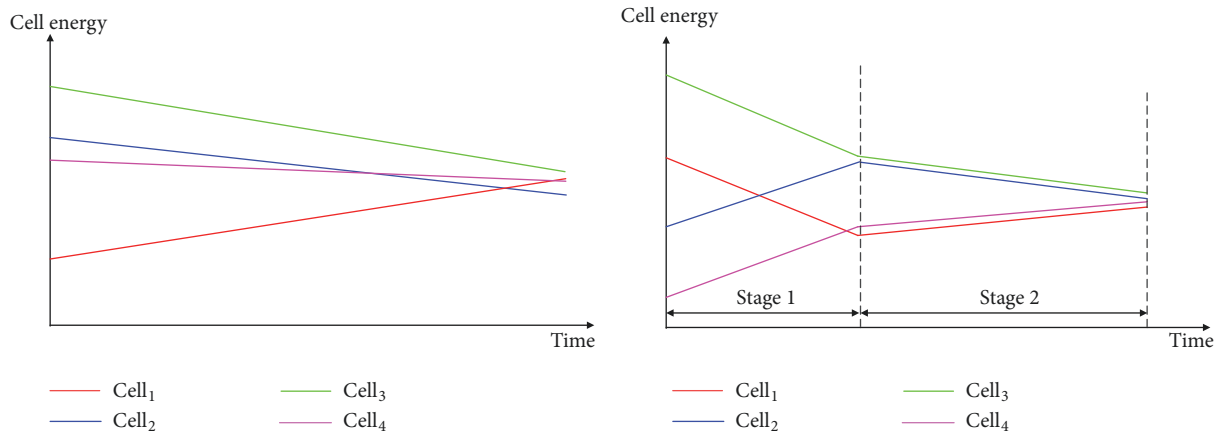

(a) Equalization process of BMMEEC

(b) Equalization process of the circuit in [23]

Figure 12: Balancing process comparison between BMMEEC and the circuit in [23].

in unnecessary energy transfer. In contrast, in the equalization process of the BMMEEC, only one termination criterion is needed and no unnecessary energy transfer exists. This simplifies the control and avoids extra equalization process.

4.5. Simulation Results in Three Equalization States under Clock Signals. All the results above are obtained when switches are actuated by ideal gating signals. However, in practical applications, control signals usually cannot reach such a precise level. Consequently, a 40KHz clock signal is applied for switches control and every 20 sequent clock cycles are regarded as one operation cycle. Consequently, the original 4000 Hz gating signal is replaced by a 1000 Hz square wave signal and a 40 kHz clock signal is used as a counting signal. The former is used for switch control as the gating signal and the latter is used for counting. The clock signal divides one square wave cycle into 10 parts. The duty cycle of each switch is changed by adjusting the number of conduction cycles of each switch every 20 clock cycles. Switches are actuated for 18, 24, and 30 clock cycles in every operation cycle until the variance of the SOC reaches the minimum value. Set the currents measured by the four ammeters to be $I1'$, $I2'$, $I3'$, and $I4'$. Figure 13 shows the corresponding waveforms of $I1'$, $I2'$, $I3'$, and $I4'$.

Figures 14(a), 14(b), and 14(c) illustrate the waveforms of the four-cell SOC in the idle state, charging state, and discharging state, respectively. Figure 14 indicates that, in the idle state, the equalization completes at 86.68s. Moreover, the battery string is charged in the charging state at 20V and 7A and the equalization completes at 84.36s. Furthermore, the battery string in the discharging state is discharged at 15V and 7A and the equalization completes at 92.42s. Table 4 displays the corresponding data.

Figure 14(a) shows that there exist deviations from Figure 11, which is caused by discrete control signals. The change in the slope of the SOC waveform indicates that the energy stored by the inductor of the equalizer flows back to the battery string after the end of control. Figure 14(b) demonstrates that, in the charging state, the cell with the lower SOC is charged faster, while the battery with the lower SOC is slowly charged or nearly is not charged. After reaching the equalization, the SOC of each battery changes uniformly. Compared with the idle state, more energy is involved in the equalization because of the external power source; hence the spent time on the equalization decreases. Therefore, it is concluded that the BMMEEC can avoid overcharging of the battery string. Similarly, Figure 14(c) demonstrates that, in the discharging state, the cell with higher SOC is discharged faster, while the battery with lower SOC is slowly charged or nearly is not discharged. After reaching the equalization, the SOC of each battery changes uniformly, which indicates that the BMMEEC can avoid overcharging of the battery. However, compared to the idle state equalization, a portion of the balancing energy is consumed by the load causes; hence the equalization time increases.

5. Conclusion and Further Work

Based on the inductor equalizer, an equalization circuit for the battery energy, called the BMMEEC, is proposed in

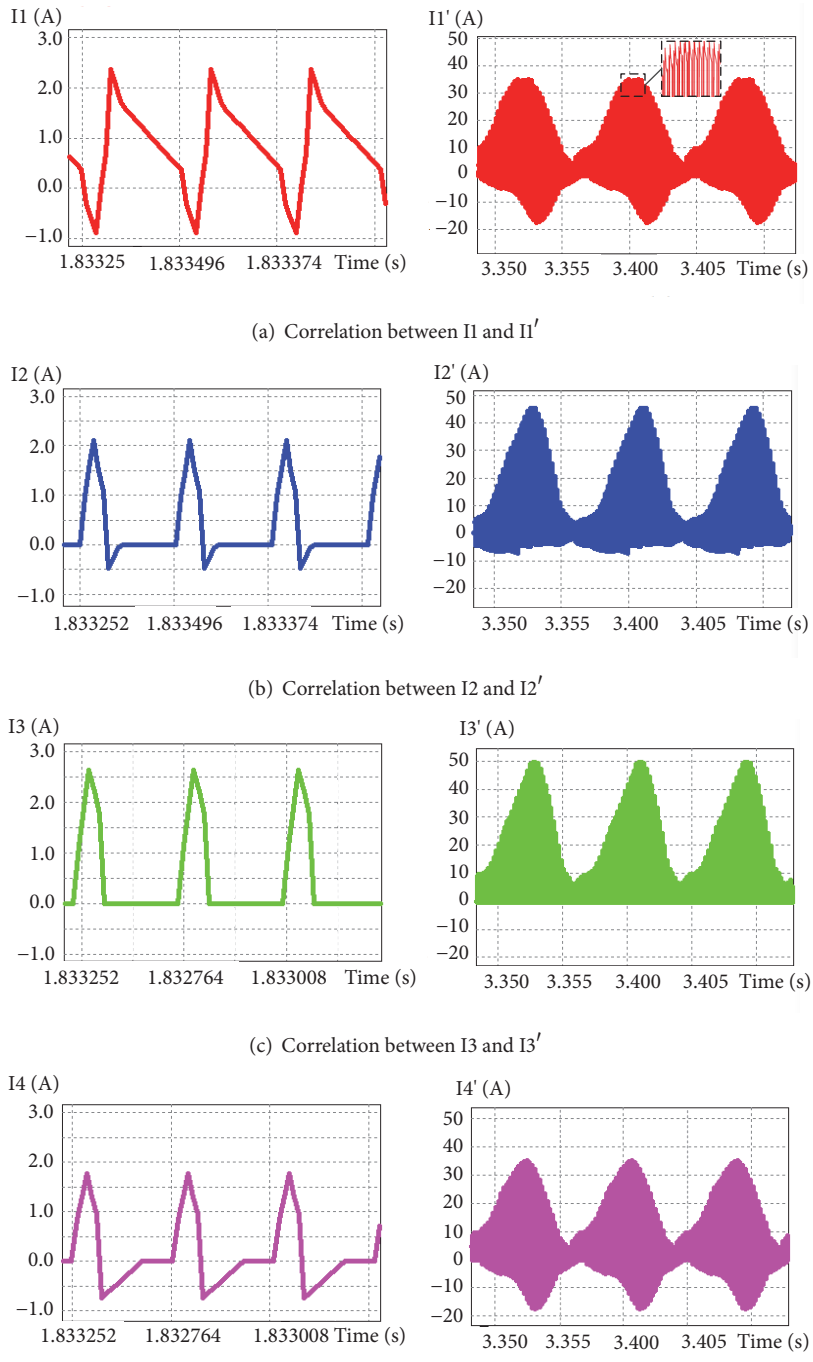

Figure 13: Correlation between current waveforms for two driven signals.

the present study. Then, the corresponding mathematical model deduction and simulation verifications are presented. Moreover, the CISGM model is developed for the mathematical description and control analysis of the BMMEEC and the feasible control is obtained by solving the model's Nash Equilibrium. An equivalent simulation model of the four-cell equalization is established in the PISM. In order to justify the CISGM during the simulation, the variation of the operational data, balancing current and battery SOC, tallied with the mathematical descriptions of the BMMEEC. It is found that four cells' SOCs are nearly identical, which verifies the control validation. Moreover, the simulation results demonstrate that the application of the BMMEEC prevents the long-period charging-discharging cycles for involved cells so that the SOC of each cell moves directly forward in harmony. It is found that the BMMEEC has the

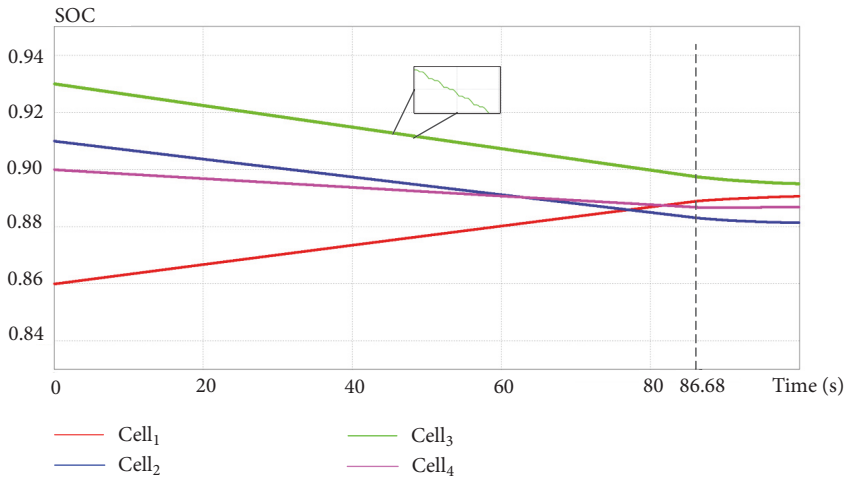

(a) SOC waveform in idle state

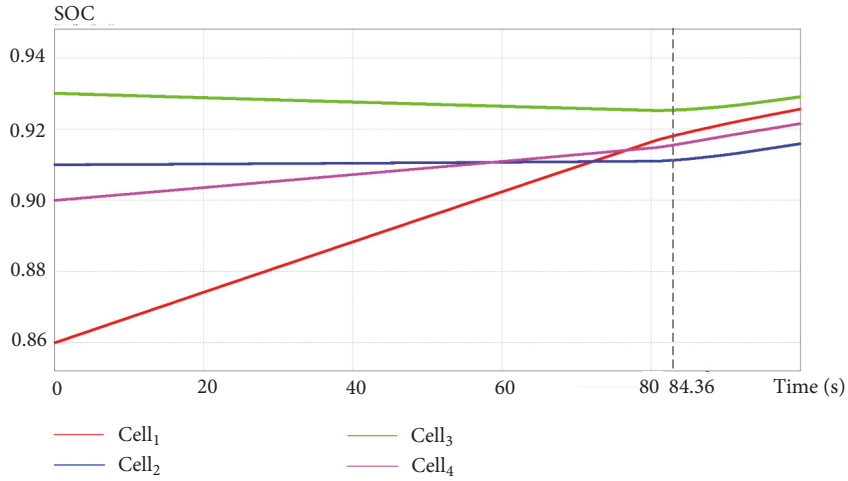

(b) SOC waveform in charging state

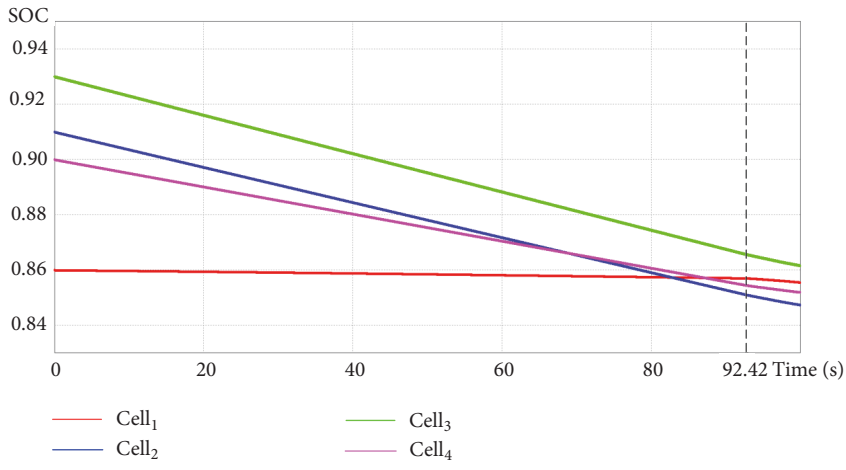

(c) SOC waveform in discharging state

Figure 14: SOC waveform for clock signals.

modularized circuit topology and the mutually independent working principle, compared with other inductor equalizers. Furthermore, it is observed that the control complexity of the BMMEEC has a linear correlation with the cell number. However, further studies are required. The simulations results have a certain deviation from the ideal equalization results, and the scale of the simulation equalization circuit was limited to four cells.

It is intended to expand the research in the following parts, in the near future: (1) investigate the relationship between the equalization deviation and parameters of the BMMEEC and describe the influence of the main factors on the quantity of the deviation. (2) Expand the string equalization of the simulation battery to larger scales, while controlling the voltage stress on each equalizer. (3) Perform the practical experiments to test the actual performance of the BMMEEC.

Data Availability

The PSIM11 simulation data used to support findings of this study are available from the corresponding author upon request.

Conflicts of Interest

The authors declare no conflicts of interest.

Authors' Contributions

Jiayu Wang developed and exploited the mathematical model for the multi-inductor battery energy equalization circuit and carried out simulations. Shuailong Dai designed the topology of the proposed circuit and polished the manuscript. Xi Chen, Xiang Zhang, and Zhifei Shan finalized and polished the manuscript.

Acknowledgments

This work was partially supported by the National Innovation and Entrepreneurship Training Program for College Students 201711075009.

References

[1] M. A. Hannan, M. M. Hoque, S. E. Peng, and M. N. Uddin, "Lithium-Ion battery charge equalization algorithm for electric vehicle applications," *IEEE Transactions on Industry Applications*, vol. 53, no. 3, pp. 2541–2549, 2017.

[2] H. Farzin, M. Fotuhi-Firuzabad, and M. Moeini-Aghtaie, "A practical scheme to involve degradation cost of lithium-Ion batteries in vehicle-to-grid applications," *IEEE Transactions on Sustainable Energy*, vol. 7, no. 4, pp. 1730–1738, 2016.

[3] P. Thounthong, S. Sikkabut, P. Mungporn et al., "DC bus stabilization of Li-Ion battery based energy storage for a hydrogen/solar power plant for autonomous network applications," *IEEE Transactions on Industry Applications*, vol. 51, no. 4, pp. 2717–2725, 2015.

[4] Y.-H. Chiang, W.-Y. Sean, C.-H. Wu, and C.-Y. Huang, "Development of a converterless energy management system for reusing automotive lithium-ion battery applied in smart-grid balancing," *Journal of Cleaner Production*, vol. 156, pp. 750–756, 2017.

[5] N. Sulaiman, M. A. Hannan, A. Mohamed, E. H. Majlan, and W. R. Wan Daud, "A review on energy management system for fuel cell hybrid electric vehicle: Issues and challenges," *Renewable & Sustainable Energy Reviews*, vol. 52, pp. 802–814, 2015.

[6] M. A. Hannan, F. A. Azidin, and A. Mohamed, "Hybrid electric vehicles and their challenges: a review," *Renewable & Sustainable Energy Reviews*, vol. 29, pp. 135–150, 2014.

[7] M. A. Hannan, M. M. Hoque, A. Mohamed, and A. Ayob, "Review of energy storage systems for electric vehicle applications: Issues and challenges," *Renewable & Sustainable Energy Reviews*, vol. 69, pp. 771–789, 2017.

[8] M. A. Hannan, M. M. Hoque, P. J. Ker, R. A. Begum, and A. Mohamed, "Charge equalization controller algorithm for series-connected lithium-ion battery storage systems: modeling and applications," *Energies*, vol. 10, no. 9, p. 1390, 2017.

[9] M. M. Hoque, M. A. Hannan, A. Mohamed, and A. Ayob, "Battery charge equalization controller in electric vehicle applications: a review," *Renewable & Sustainable Energy Reviews*, vol. 75, pp. 1363–1385, 2017.

[10] Y. Ma, Y. Chen, X. Zhou, and H. Chen, "Remaining useful life prediction of lithium-ion battery based on gauss-hermite particle filter," *IEEE Transactions on Control Systems Technology*, vol. 3, pp. 1–8, 2018.

[11] L. Zheng, J. Zhu, G. Wang, D. D.-C. Lu, and T. He, "Lithium-ion battery instantaneous available power prediction using surface lithium concentration of solid particles in a simplified electrochemical model," *IEEE Transactions on Power Electronics*, vol. 33, no. 11, pp. 9551–9560, 2018.

[12] N. Sulaiman, M. A. Hannan, A. Mohamed, P. J. Ker, E. H. Majlan, and W. R. Wan Daud, "Optimization of energy management system for fuel-cell hybrid electric vehicles: issues and recommendations," *Applied Energy*, vol. 228, pp. 2061–2079, 2018.

[13] T. Stuart and W. Zhu, "Fast equalization for large lithium ion batteries," *IEEE Aerospace and Electronic Systems Magazine*, vol. 24, no. 7, pp. 27–31, 2009.

[14] S. Bergvik and L. Bjorkstrom, "Prolonged useful life and reduced maintenance of lead-acid batteries, by means of individual cell voltage regulation," in *Proceedings of the International Telecommunications Energy Conference*, IEEE, 1984.

[15] C. Pascual and P. T. Krein, "Switched capacitor system for automatic series battery equalization," in *Proceedings of the 1997 IEEE 12th Applied Power Electronics Conference*, pp. 848–854, February 1997.

[16] A. C. Baughman and M. Ferdowsi, "Double-tiered switched-capacitor battery charge equalization technique," *IEEE Transactions on Industrial Electronics*, vol. 55, no. 6, pp. 2277–2285, 2008.

[17] K.-M. Lee, S.-W. Lee, Y.-G. Choi, and B. Kang, "Active balancing of Li-Ion battery cells using transformer as energy carrier," *IEEE Transactions on Industrial Electronics*, vol. 64, no. 2, pp. 1251–1257, 2017.

[18] A. G. Xu, S. J. Xie, and X. B. Liu, "Dynamic voltage equalization for series-connected ultracapacitors in EV/HEV applications," *IEEE Transactions on Vehicular Technology*, vol. 58, no. 8, pp. 3981–3987, 2009.

[19] C.-H. Kim, M.-Y. Kim, H.-S. Park, and G.-W. Moon, "A modularized two-stage charge equalizer with cell selection switches for series-connected lithium-ion battery string in an HEV," *IEEE Transactions on Power Electronics*, vol. 27, no. 8, pp. 3764–3774, 2012.

[20] S. H. Park, K. B. Park, H. S. Kim, G. W. Moon, and M. J. Youn, "Single-magnetic cell-to-cell charge equalization converter with reduced number of transformer windings," *IEEE Transactions on Power Electronics*, vol. 27, no. 6, pp. 2900–2911, 2012.

[21] X. Wang, K. W. E. Cheng, and Y. C. Fong, "Non-equal voltage cell balancing for battery and super-capacitor source package management system using tapped inductor techniques," *Energies*, vol. 11, no. 5, p. 1037, 2018.

[22] K. Nishijima, H. Sakamoto, and K. Harada, "PWM controlled simple and high performance battery balancing system," in *Proceedings of the IEEE Power Electronics Specialists Conference*, vol. 2000, IEEE Xplore.

[23] N. H. Kutkut, H. Wiegman, and A. Marion, "Modular battery charge equalizers and method of control," United States Patent 6150795, 2000.

[24] J. Zhao, J. Jiang, and L. Niu, "A novel charge equalization technique for electric vehicle battery system," in *Proceedings of the 5th International Conference on Power Electronics and Drive Systems, PEDS 2003*, pp. 853–857, November 2003.

[25] Y. Lee, C. Tsai, Y. Ko, and M. Cheng, "Charge equalization using quasi-resonant converters in battery string for medical power operated vehicle application," in *Proceedings of the 2010 International Power Electronics Conference (IPEC - Sapporo)*, pp. 2722–2728, Sapporo, Japan, June 2010.

[26] P. A. Cassani and S. S. Williamson, "Feasibility analysis of a novel cell equalizer topology for plug-in hybrid electric vehicle energy-storage systems," *IEEE Transactions on Vehicular Technology*, vol. 58, no. 8, pp. 3938–3946, 2009.

[27] P. A. Cassani and S. S. Williamson, "Design, testing, and validation of a simplified control scheme for a novel plug-in hybrid electric vehicle battery cell equalizer," *IEEE Transactions on Industrial Electronics*, vol. 57, no. 12, pp. 3956–3962, 2010.

[28] X. Guo, L. Kang, Z. Huang, Y. Yao, and H. Yang, "Research on a novel power inductor-based bidirectional lossless equalization circuit for series-connected battery packs," *Energies*, vol. 8, no. 6, pp. 5555–5576, 2015.

[29] J. R. Marden and J. S. Shamma, "Game theory and control," *Annual Review of Control, Robotics, and Autonomous Systems*, vol. 1, no. 1, pp. 105–134, 2018.

[30] C. Yufei, *Lithium battery pack charging equilibrium game model and control strategy, [PhD Diss.]*, 2015.

[31] R. W. Ferrero, S. M. Shahidehpour, and V. C. Ramesh, "Transaction analysis in deregulated power systems using game theory," *IEEE Transactions on Power Systems*, vol. 12, no. 3, pp. 1340–1347, 1997.

[32] N. Li, J.-F. Martinez-Ortega, and V. H. Diaz, "Distributed power control for interference-aware multi-user mobile edge computing: a game theory approach," *IEEE Access*, vol. 6, pp. 36105–36114, 2018.

[33] G. Saloner, "Modeling, game theory, and strategic management," *Strategic Management Journal*, vol. 12, no. 2 S, pp. 119–136, 1991.

[34] R. B. Myerson, *Game Theory: Analysis of Conflict*, Harvard University Press, 1997.

[35] Y. Çadirci and Y. Özkazanç, "Microcontroller-based on-line state-of-charge estimator for sealed lead-acid batteries," *Journal of Power Sources*, vol. 129, no. 2, pp. 330–342, 2004.

[36] M. A. Hannan, M. S. H. Lipu, A. Hussain, and A. Mohamed, "A review of lithium-ion battery state of charge estimation and management system in electric vehicle applications: Challenges and recommendations," *Renewable & Sustainable Energy Reviews*, vol. 78, pp. 834–854, 2017.

[37] M. S. H. Lipu, M. A. Hannan, A. Hussain et al., "A review of state of health and remaining useful life estimation methods for lithium-ion battery in electric vehicles: challenges and recommendations," *Journal of Cleaner Production*, vol. 205, pp. 115–133, 2018.

[38] M. S. H. Lipu, M. A. Hannan, A. Hussain, M. H. M. Saad, A. Ayob, and F. Blaabjerg, "State of charge estimation for lithium-ion battery using recurrent NARX neural network model based lighting search algorithm," *IEEE Access*, vol. 6, pp. 28150–28161, 2018.

[39] M. A. Hannan, M. S. H. Lipu, A. Hussain, M. H. Saad, and A. Ayob, "Neural network approach for estimating state of charge of lithium-ion battery using backtracking search algorithm," *IEEE Access*, vol. 6, pp. 10069–10079, 2018.